



Cloud and rain liquid water statistics in the CHUVA campaign



Alan J.P. Calheiros, Luiz A.T. Machado

Instituto Nacional de Pesquisas Espaciais, Centro de Previsão de Tempo e Estudos Climáticos, Cachoeira Paulista, SP, Brazil

ARTICLE INFO

Article history:

Received 4 April 2013

Received in revised form 9 March 2014

Accepted 10 March 2014

Available online 19 March 2014

Keywords:

Cloud liquid water

Cloud types

Droplet size distribution

Radar

Radiometer

ABSTRACT

The purpose of this study is to present statistics related to the integration of cloud and rain liquid water and the profiles for different cloud types and regimes. From 2010 to 2012, the CHUVA project collected information regarding cloud and rain characteristics in different precipitation regimes in Brazil. CHUVA had four field campaigns between 2010 and 2011, located in the North, Northeast and Southeast regions of Brazil, covering the semi-arid, Amazon, coastal and mountain regions. The synergy of several instruments allowed us to classify rain events and describe the cloud processes regionally. Microwave radiometers, LiDAR, radar, and disdrometers were employed in this study. The rain type classification was made using vertical profiles of reflectivity (VPR) and polarimetric variables from dual polarization radar (XPOL). The integrated liquid water (ILW_C) for non-precipitating clouds was retrieved with a microwave ground-based radiometer using a neural network. For rainy conditions, the profiles from the rain liquid water content (LWC_R) and their integrated (ILW_R) properties were estimated by Micro Rain Radar (MRR) and XPOL VPRs. For non-precipitating clouds, the ILW_C values were larger for the sites in tropical regions, in particular near the coast, than for Southeast Brazil. For rainy cases, distinct LWC_R profiles were observed for different rain classifications and regions. The differences are small for low rain rates and a distinction between different rainfall regimes is more evident for high rain rates. Vale and Belém clouds present the deepest layers and largest convective rain rates. The clouds in the Southeast region of Brazil (Vale do Paraíba) and North region (Belém) showed the largest reflectivity in the mixed and glaciated layers, respectively. In contrast, the Northeast coastal site (e.g. Fortaleza) showed larger values in the warm part of the clouds. Several analyses are presented, describing the cloud processes and the differences among the cloud types, rain rates and regimes.

© 2014 Elsevier B.V. All rights reserved.

1. Introduction

Clouds cover approximately 68% of the Earth; therefore, it is essential to understand the physical properties of clouds in order to diagnose the Earth's energy and water balance (Rossow and Shiffer, 1999). Atmospheric water is found as vapor (gas phase), cloud and rain liquid water (liquid phase) and different types of ice, such as snow and hail (solid phase). The significant variability of hydrometeors is due to the complex atmospheric physical processes that directly impact the weather conditions and climate. For example, the quantity of water in the clouds influences the amount of

latent heat and, consequently, the upward and downward motions within the cloud (Zhao and Carr, 1997). The energy balance is also strongly dependent on the amounts of water and ice in the clouds (Crewell and Löhnert, 2003; Zhao and Weng, 2002), which directly influence the climate. However, as mentioned by Löhnert et al. (2001), the lack of information concerning these complex processes, especially with respect to cloud microphysics, has limited the available parameterizations in high-resolution numerical models. Unlike other meteorological parameters, the liquid water content of clouds is not measured operationally, and there is little information about the variability of the average properties. The importance of this knowledge goes beyond forecasting and climate modeling, to the nowcasting of severe events (Greene and Clark, 1972).

E-mail addresses: alan.calheiros@cptec.inpe.br (A.J.P. Calheiros), luz.machado@cptec.inpe.br (L.A.T. Machado).

According to Pruppacher and Klett (1997), liquid water content varies considerably among clouds, from approximately 0.2 g m^{-3} in the initial stage of cumulus cloud development up to 14 g m^{-3} during severe storms. Cotton et al. (2010) list a series of characteristics associated with different cloud types, showing that liquid water content varies significantly. For example, stratus cloud liquid water presents values of approximately 0.05 to 0.25 g m^{-3} , although cases exist in which these values range up to 0.6 g m^{-3} . This is in agreement with Hogan et al. (2005), based on the synergistic use of many active sensors, although the maximum found for ordinary cumulus clouds was 1 g m^{-3} . However, Lawson and Blyth (1998) found a large variability. Nonetheless, this value is easily exceeded by systems with large vertical development, such as cumulonimbus, which can have values above 1.5 g m^{-3} .

Atmospheric remote sensing by weather radar is one of the most applicable methodologies for determining those quantities around the world, since the high cost of in situ measurements (e.g. aircraft) is limited to short periods for some specific regions of the world. Atlas (1954) and Donaldson (1955) were among the first to use active remote sensing to study cloud liquid water content and precipitation. Even so, according to Hagen and Yuter (2003), relationships between radar reflectivity and liquid water content (Z -LWC), a very useful type of parameterization, are not as frequently considered as Z -R relations (radar reflectivity (Z) and rain rate (R); Michaelides et al., 2009). Recently, Zhao et al. (2013) showed different relationships based on polarimetric variables to estimate the rainwater content, as well as the effects of attenuation on X-band radar retrievals, also described by Eccles and Mueller (1971). Meywerk et al. (2005) showed several techniques that allow the estimation of liquid water content, in addition to the synergy between the various collocated instruments. As reported by Ebell et al. (2010), the use of a ground-based radiometer may assist in the estimation performed by cloud radar. The use of passive microwave radiometers to estimate the integrated liquid water (ILW_C) for non-precipitating clouds has been widely applied (Peter and Kämpfer, 1992; Liljegren et al., 2001; Ware et al., 2003; Westwater et al., 2005; Mätzler and Morland, 2009; Karmakar et al., 2011). Following Crewell and Löhnert (2003), the accuracy of these ILW_C retrievals by radiometers can achieve 16 g m^{-2} , depending on the calibration and weather conditions (e.g. non-rainy events). Nonetheless, the major difficulty is the partitioning of cloud and rain water content within the same cloud. Based on studies of the polarization difference signal in raindrops performed by Czekala and Simmer (1998) and Czekala et al. (2001), Saavedra et al. (2012) found mean squared errors of 0.144 mm for cloud and 0.052 mm for rain liquid water content during precipitation events using active and passive sensors.

The goal of this study is to determine the water content of precipitating and non-precipitating clouds and the liquid water profiles for different cloud types and regions in Brazil. The data employed in this study were acquired during four field experiments throughout Brazil during the CHUVA¹ [Cloud process of the main precipitation system in Brazil: a contribution to cloud resolving Modeling And to the Global Precipitation Measurement (GPM, Smith et al., 2007)] project. This work

discusses the main differences among the profiles of liquid water content and the corresponding integrated liquid water for the various precipitation regimes over the continental and coastal regions in tropical or subtropical latitudes. Also, this study discusses differences among measurements from different sensors and the limitations and errors associated with each type of measurement.

2. Data and methods

2.1. The CHUVA project

The field campaigns of CHUVA focused on understanding the radiative and microphysical processes of continental clouds over Brazil. For a detailed description of the CHUVA project see Machado et al. (in press). The CHUVA field experiments were conducted in different places with different weather patterns, using the same measurement strategy (described below) and instruments to study the precipitation regimes. During the experiments, polarimetric and vertically pointing radars, microwave radiometers, disdrometers, GPS, radiosondes and various other instruments were used. One of the main objectives was to minimize the uncertainties in satellite rainfall estimation as reported by Stephens and Kummerow (2007). Precipitation from warm clouds, based on scattering algorithms, is not retrieved. Besides, information about the atmospheric states as well as the cloud and precipitation structures is very important to improve precipitation estimation. The characterization of different rainy clouds in different regions of Brazil would assist the development or improvements of satellite-based rainfall estimation algorithms.

2.2. Measurement strategy

The data used in this study were obtained from field experiments of the CHUVA project, conducted between March 2010 and December 2011, over four regions of Brazil. Two experiments focused on the characterization of warm clouds, the first of which was performed in Alcântara in the state of Maranhão from March 3 to April 15, 2010, and the second of which was held in Fortaleza in the state of Ceará from April 4 to May 1, 2011. Both are located on the coast of Northeast Brazil. The third field experiment was conducted during the month of June in Belém, in the state of Pará in the North region of Brazil. From November 1 to December 21, 2011, the CHUVA project was held in Southeast Brazil in Vale do Paraíba in the state of São Paulo. Fig. 1 shows the geographical position of each field experiment in the CHUVA project. A schematic representation of the instrument distribution was described by Machado et al. (in press). This study uses the data from three sites, as described below:

- *Main site*: This site had instruments to measure clouds and rainfall in high temporal resolution. The following instruments were employed in this study: PARSIVEL (PARTicle Size and VELOCITY) and Joss-Waldvogel (JWD) disdrometers, tipping bucket rain gauges, MP-3000A microwave radiometer, LiDAR and Micro Rain Radar.
- *RADAR site*: X-band dual polarization radar was run with two scan strategies including a volume scan and Height Indicator Range (RHI) every 6–10 min. The latter was oriented over the

¹ Meaning rain in Portuguese.

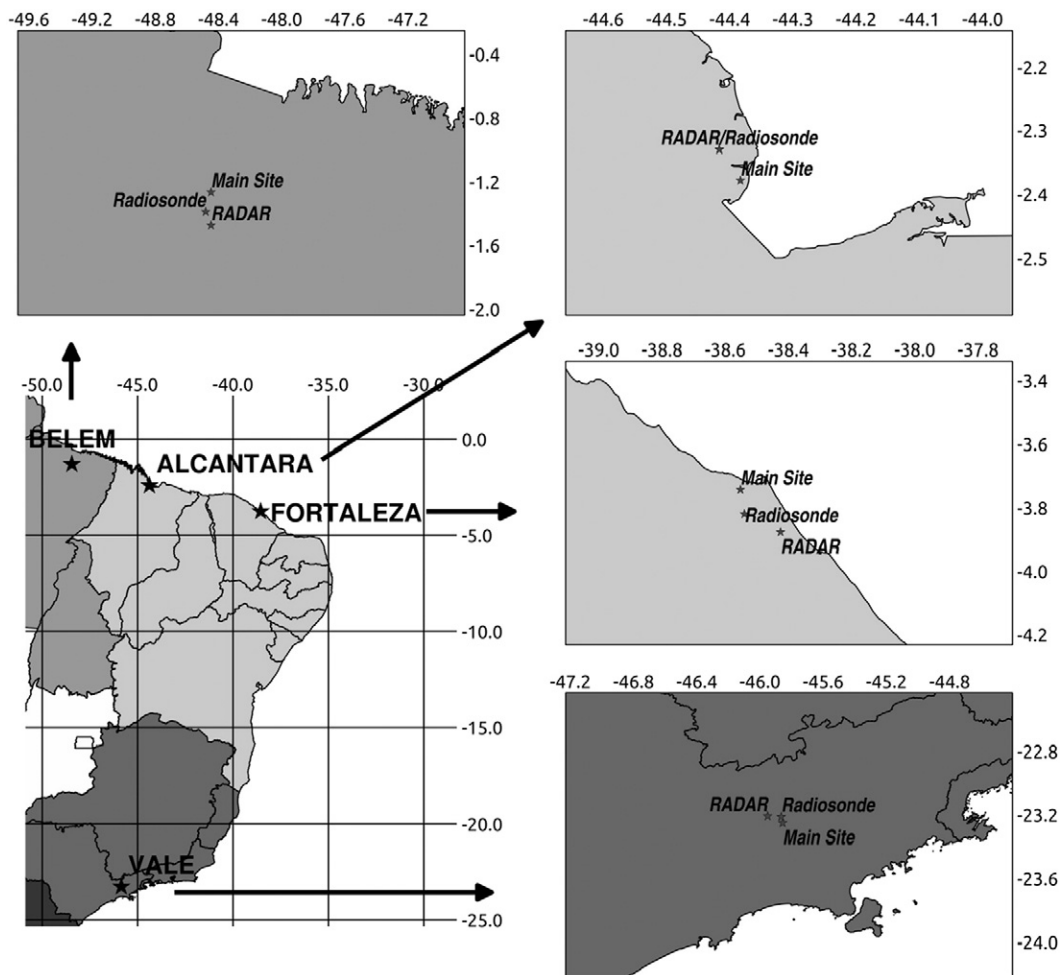


Fig. 1. The site locations for the CHUVA campaign from 2010 to 2012. The three studied regions of Brazil are represented by colors: light gray (Northeast), gray (North) and dark gray (Southeast).

main site, and the distances between these sites were: Alcântara (6.5 km), Fortaleza (20.6 km), Belém (23.3 km) and Vale do Paraíba (10.8 km);

- **Radiosonde site:** RS-92 radiosondes were released at least twice a day, but in most experiments a temporal resolution of 6 h was adopted (00, 06, 12, and 18 GMT). The distances between the radiosonde and main sites were: Alcântara (6.5 km), Fortaleza (8.7 km), Belém (14.3 km) and Vale do Paraíba (4.5 km).

The four campaigns were located in regions with different frequencies of synoptic systems; see [Satyamurty et al. \(1998\)](#). The campaigns occurred during the rainy season of each region. Below we describe the synoptic situation during each campaign:

- **Alcântara:** The synoptic conditions at the beginning of the experiment did not favor the formation of rain clouds. During the first two weeks only a few rain events were reported; this anomalous situation was associated with a Southern Hemisphere (SH) anti-cyclonic flow which evolved into a high pressure area in the upper levels of the atmosphere. In the second half of the Alcântara campaign, the synoptic condition drastically changed; an

Upper Level Cyclonic Vortex (ULCV; [Kousky and Gan, 1981](#)) moved from the Atlantic Ocean to the coast of Northeast Brazil. Large convective systems and several rainfall events were reported.

- **Fortaleza:** The synoptic situation was also associated with an ULCV; during some periods, when Fortaleza was located in the center of ULCV, subsidence was typically observed; however, the ULCV moved and the region was under the influence of the ULCV's left branch and both local and organized convection events were observed. In addition, the low- and mid-level flows favored atmospheric moisture transport from the ocean to the coast. Furthermore, the Intertropical Convergence Zone (ITCZ) was positioned further south over Northeast Brazil and brought heavy rainfall events.
- **Belém:** The rainfall events in Belém were mostly associated with local convection and several squall line events. The second half of the campaign had more developed rainfall events than the first one. Two typical squall line events were reported, one formed by sea breezes and the other formed to the east, moving westward parallel to the coast.
- **Vale do Paraíba:** The main rainfall systems during the campaign were caused by the penetration of cold fronts,

local convection and organized mesoscale systems. The presence of a 500 hPa trough to the east (first half of the period) and west (second part) was responsible for the atmospheric moisture flow over the region and, consequently, the precipitation regime. Several thunderstorm events, some associated with hail, were reported during the campaign.

2.3. Instruments and limitations

2.3.1. Microwave radiometer

To analyze the liquid water content in non-precipitating clouds, a ground-based microwave radiometer (MWR) was used (Radiometrics MP-3000A, Ware et al., 2013). This instrument measures passive radiation at microwave wavelengths in 35 channels, ranging from 22 to 30 GHz (21 channels), associated with the emission by water vapor, and from 51 to 59 GHz (14 channels), related to the emission by oxygen molecules. Details regarding the physical principles can be found in Westwater (1993), and Westwater et al. (2005). The MWR is a robust instrument designed to handle the most diverse weather conditions (Cadeddu et al., 2013; Campos et al., in press). The most sensitive structural part of the instrument is the radome (Rose et al., 2005) through which the radiation passes before reaching the receiver. Problems associated with accumulation of liquid water on the radome may produce erroneous estimations of atmospheric parameters. The radome is built with a hydrophobic material and fitted with a Superblower, since the presence of water during precipitation events influences the signal; however, after rainfall events anomalous values were reported, generating unreliable measurements. Accurate measurements are reported during heavy precipitation using off-zenith observation and retrieval methods (Cimini et al., 2011; Xu et al., 2013; Ware et al., 2013), but these methods were not applied for this study. Therefore, only the measurements during non-raining events were considered. Another uncertainty in the measurements is related to the errors in instrument calibration (Skou and Vine, 2006). To avoid these problems, calibration was performed using liquid nitrogen (Hardy, 1973) before each campaign, and during the measurements, tip calibration was applied (Han and Westwater, 2000; Cimini et al., 2003). Other uncertainties associated with the beam filling were described by Hewison (2006).

2.3.2. Disdrometer

During the experiments various rain gauges were collocated with the disdrometers. Generally, two types of disdrometers were employed, the PARSIVEL (Löffler-Mang and Joss, 2000) and JWD (Joss and Waldvogel, 1967); only PARSIVEL measurements were performed for all the sites, so it was chosen among the disdrometers to define the precipitation in this study. Thus, the rain rate, radar reflectivity and liquid water content were estimated based on the size and terminal velocity of hydrometeors passing through the detection area of the laser (54 cm²). However, a filter to avoid raindrops associated with unrealistic terminal velocities was applied (Tokay et al., 2013); it removed about 25% of the detectable particles (Jaffrain and Berne, 2011). Other limitations for PARSIVEL measurements were reported by Tokay et al. (2013); the equipment tends to underestimate the smallest and overestimate the largest raindrops compared to other disdrometer models that are considered more efficient by the authors, e.g. JWD. In addition, unrealistic measurements

associated with LWC larger than 15 g m⁻³ were removed. The rain liquid water content was also computed using JWD (when available); the results were very similar, even if the mean droplet size distributions (DSD) from both were sometimes different.

2.3.3. Radar

For cases associated with rain clouds, the rain integrated liquid water content (ILW_R) and the rain liquid water content (LWC_R) profiles were determined using the vertical profiles of reflectivity (VPR) of the two radar systems, Micro Rain Radar (MRR, Peters et al., 2005) and an X-band dual polarization at 9.365 GHz (XPOL) radar (mobile Selex Meteor 50DX for all sites except Alcântara, where a fixed EEC X was employed). Both radar systems suffer rain attenuation effects (see Peters et al., 2010; Doviak and Zrníc, 1993). With respect to the XPOL, the strategy to place the main site a short distance from the radar site minimized the effects of attenuation. Nevertheless, depending on the intensity of precipitation, attenuation can be very strong, particularly for MRR. Additionally, attenuation corrections were applied to both radars. In the MRR, a path-integrated attenuation (PIA) was used, according to Peters et al. (2010). However this correction is only applied to PIA ≤ 10 dB, and for this reason uncorrected data were not employed in the rainwater analyses. Moreover, updrafts and downdrafts can cause significant variations in the raindrop size distribution estimates, which are directly reflected in the reflectivity retrieved by the MRR (Peters et al., 2005). Hence, the presence of deep convection can cause erroneous liquid water content in MRR measurements; therefore, MRR was not used for this purpose.

The CHUVA XPOL radar attenuation is discussed by Schneebeli et al. (2012). The attenuation correction was based on the algorithm provided by the manufacturer employing the ZPHI relation as proposed by Testud et al. (2000). As mentioned, for Alcântara a different radar system was employed; however, a specific bias adjustment (12 dBZ) was applied using a collocated MRR radar coupled with the ADMIRARI system (Battaglia et al., 2011).

2.3.4. LiDAR

Another instrument used during the Fortaleza campaign was a LiDAR (Light Detection And Ranging, LB10 Raymetrics D-200). This equipment provided information about the cloud geometrical thickness from the vertical variation of the backscattered signal using a green wavelength (Bourayou et al., 2011). The LiDAR measured from the surface up to around 30 km with 7.5 m vertical resolution, and a temporal resolution of 20 Hz averaged in 1 min. All profiles were stored in the same 24 hour matrix for simultaneous treatment; thereafter, a threshold and binary erosion using digital image processing (Gonzalez et al., 2009) was applied to determine only the cloud signal.

2.4. The liquid water calculation

The direct measurement of the total liquid water content in a given cloud at any given time can only be performed by using several aircrafts, which must simultaneously profile the cloud. However, since only ground-based remote sensing instrumentation was used in this experiment, specifying the properties of a cloud mixed layer (such as thickness of the

Table 1
Instrument synergy employed for specific variable calculation.

Variable	Instrument synergy
ILW _C (mm)	MWR (retrieval and measurements) and disdrometer (employed to filter out rainy events)
ILW _{Adia} (mm)	Pressure, temperature and humidity from RS92 radiosonde and disdrometer (employed to filter out rainy events)
Cloud thickness (m)	LiDAR and disdrometer (employed to filter out rainy events)
ILW _R (XPOL) (mm)	XPOL and disdrometer (employed to define rainy events) and radiosonde (to define the melting layer)
ILW _R (MRR) (mm)	MRR and disdrometer (employed to define rainy events) and radiosonde (to define the melting layer)
Cloud classification	XPOL (including polarimetric variables) and radiosonde (to define the melting and lifting condensation levels)
LWC _R (mm)	XPOL and disdrometer (employed to define rainy events and Z–LWC relationship)
VIL (mm)	XPOL and disdrometer (employed to define rainy events and Z–LWC relationship) and radiosonde (to define the integration layers)
DSD (m ⁻³ mm ⁻¹)	Disdrometer PARSIVEL and XPOL (including polarimetric variables for cloud classification)

layer or particle concentrations and densities), was not possible. Thus, we chose to perform only two distinct analyses, one for non-precipitating events and another for clouds with rain, describing the cloud characteristics below the melting layer. The rainfall events for each site were identified as the events whose precipitation, as measured by disdrometer, was greater than 0.1 mm h⁻¹ (Tokay et al., 2001). Furthermore, all data used in the rain vertical analysis were collocated with respect to the XPOL and MRR measurements. The instruments employed for the calculation of each variable are listed in Table 1.

2.4.1. Non-precipitating clouds

During the CHUVA project experiments, the MWR performed continuous thermodynamic soundings in all weather conditions with a temporal resolution higher than 6 min. This measurement provides the temperature (K), relative humidity (%) and liquid water (g m⁻³) profiles up to 10 km in height, as well as the water vapor (mm) and liquid water (mm) integrations. The retrieval of these parameters was performed using neural networks (Solheim et al., 1998). Historical radiosonde data sets from locations near the sites of each campaign were used for network training provided by the manufacturer. The ILW_C retrieval using MWR was applied only for conditions without rain. Furthermore, another filter was applied to avoid the presence of raindrops in the clouds and over the radome; ILW_C values were not estimated for a period of 30 min before and after precipitation. According to Löhnert and Crewell (2003), the formation of raindrops can affect the brightness temperatures in the microwave band. Using similar equipment, Won et al. (2009) showed that approximately 30 min before rain events there is a considerable increase in brightness temperature for different channels, probably associated with raindrop formation. This is in agreement with Beard and Ochs (1993), where the authors show that the process of rain formation in warm clouds takes 10 to 30 min. Furthermore, the effect of raindrops over the radome after the rain could be observed for all campaigns during CHUVA.

Table 2

Z–LWC and Z–R relationships observed for each site during the CHUVA campaign. r^2 is the coefficient of determination.

Site	Z–LWC	r^2	Z–R	r^2
Alcântara	$Z = 22357.6LWC^{1.44}$	0.95	$Z = 362.1R^{1.32}$	0.97
Fortaleza	$Z = 18162.7LWC^{1.45}$	0.95	$Z = 311.8R^{1.31}$	0.98
Belém	$Z = 20081.8LWC^{1.45}$	0.95	$Z = 336.1R^{1.32}$	0.97
Vale do Paraíba	$Z = 25184.5LWC^{1.56}$	0.93	$Z = 337.7R^{1.38}$	0.96

These filters removed approximately 85% of the ILW_C data greater than or equal to 0.001 mm from Fortaleza, 70% from Belém, 55% from Vale do Paraíba and 85% from Alcântara. Furthermore, a noise signal was observed in Vale related to the ambient temperature; for this reason a correction was applied using a linear fitting equation ($ILW_C = ILW_{C(\text{original})} - 0.0089 * T + 0.0454$, T is the ambient temperature in °C). Unrealistic values were observed during the wettest period in the early hours of the day, probably related to dew over the radome. To avoid this problem, measurements associated with relative humidity higher than 93% between 3 and 9 GMT were not considered for Vale. In Alcântara, unrealistic ILW_C were noted close to midday and removed. Off-zenith methods minimize errors generated by dew on the radome; however, such methods were not applied in this study.

The adiabatic ILW calculation using collocated radiosondes was applied to compare with the ILW_C retrieval using MWR. The methodology employed was the same as discussed by Ingold et al. (1998). The adiabatic liquid water content (LWC_{adia}) for each layer (h) and the integrated liquid water content (ILW_{adia}), were computed as follows:

$$LWC_{adia}(h) = (\rho_{base} - \rho_{top}) \left(\frac{h - H_{top}}{H_{top} - H_{base}} \right) C \quad (1)$$

where ρ is the saturated water vapor density (g m⁻³) at the cloud base (H_{base}) and top (H_{top}) and $C = 0.7$ is a conversion factor given in Ingold et al. (1998). Thus, the adiabatic integrated cloud liquid water is defined by the integration of LWC_{adia} in the cloud layer (relative humidity greater than 93%):

$$ILW_{adia} = \int_{H_{base}}^{H_{top}} LWC_{adia}(h) dh \quad (2)$$

In addition, the integrated water vapor using the radiosonde was also calculated. The integrated water vapor is based on the water vapor density (ρ_v) integration from the surface height (h_s) up to the level (h) where the presence of water vapor is still detectable by the radiosonde, as follows:

$$IWW = \int_{h_s}^h \rho_v(h) dh \quad (3)$$

2.4.2. Rain liquid water

The LWC_R estimated by XPOL is based on VPR, which in turn is determined by the mean reflectivity at a distance of 250 m around the main site with a vertical resolution of 200 m. Thus,

the XPOL LWC_R was estimated using the reflectivity–liquid water content power-relation ($Z = \alpha LWC^\beta$) defined by the PARSIVEL measurements (Z–LWC). This relationship was adjusted using the DSD measured by the PARSIVEL disdrometers in each site. Table 2 shows the Z–LWC relationship, as well as the Z–R, for each site during the CHUVA campaign. The equations for Z, R, and LWC for disdrometers (also applied to MRR, see Peters et al., 2005) were defined as follow:

$$Z = \int_0^\infty N(D)D^6 dD \quad (4)$$

$$R = \frac{\pi}{6} \int_0^\infty N(D)D^3 u(D) dD \quad (5)$$

where u is the terminal velocity ($m s^{-1}$), D is the rain-drop diameter (mm), and $N(D)$ is the number concentration ($m^{-3} mm^{-1}$), also called DSD. The rain liquid water content was defined by:

$$LWC = \rho_w \frac{\pi}{6} \int_0^\infty N(D)D^3 dD \quad (6)$$

ρ_w is the water density ($kg m^{-3}$).

The following equation shows the conversion of radar reflectivity from XPOL to LWC_R using a given Z–LWC relationship (Table 2).

$$LWC_R(h) = \left(\frac{Z(h)}{\alpha} \right)^{1/\beta} \quad (7)$$

where Z ($Z = 10^{(dBZ/10)}$) is the radar reflectivity ($mm^6 m^{-3}$) and h is the VPR level (resolution of 200 m), α (multiplicative factor) and β (exponent) represent the coefficient of the Z–LWC equation.

The ILW_R was defined as the amount of liquid water in the warm part of the cloud, i.e., in the layer between the cloud base and 1 km below the melting. This layer is considered to be the layer that can potentially transform into precipitation. This approach was also selected due to the bright band (BB) effect that occurs in stratiform clouds, which is characterized by a peak of reflectivity that can provide an erroneous LWC_R estimation. The sudden change of reflectivity in this layer is associated with changes in the refractive index with respect to the thickness of the water film around the melting hydrometeor (Battan, 1973; Houze, 1993). Considering that the BB thickness can reach 1 km (Battaglia et al., 2003) and the maximum of the average distances observed for each site between the 0 °C level and the peak of the BB was 0.5 km, we are assuming that the thickness between the freezing level and the BB base is close to 1 km. The ILW_R is computed, Eq. (8), as the integral of LWC_R from the lifting condensation level (computed using the radiosonde) up to 1 km below the level of 0 °C (also employing radiosonda data).

$$ILW_R(XPOL) = \int_{H_{LCL}}^{H_{0^\circ C}-1km} LWC_R(h) dh \quad (8)$$

Another parameter computed was the vertically integrated liquid water content (VIL) as defined by Greene and Clark (1972). This is a similar parameter to the ILW_R , however, in

this study we defined VIL only for the ice part of the cloud. The VIL calculation was computed for two layers, see Eq. (9); one between 0 °C and –20 °C, that we employed to describe the mixed layer and another in the layer between –20 °C and –40 °C to describe the glaciated cloud layer. As already mentioned, we are employing only ground-based remote sensing and these calculations and layers are an estimate and they are utilized only for a comparison between the different regions.

$$VIL(XPOL) = \int_{H_{0/-20^\circ C}}^{H_{-20^\circ C/-40^\circ C}} LWC_R(h) dh \quad (9)$$

With respect to MRR, the LWC_R was defined by the radar algorithm (Peters et al., 2005). For both radars, their estimations were limited to the maximum LWC observed by PARSIVEL for each site to avoid unrealistic values; thus, the

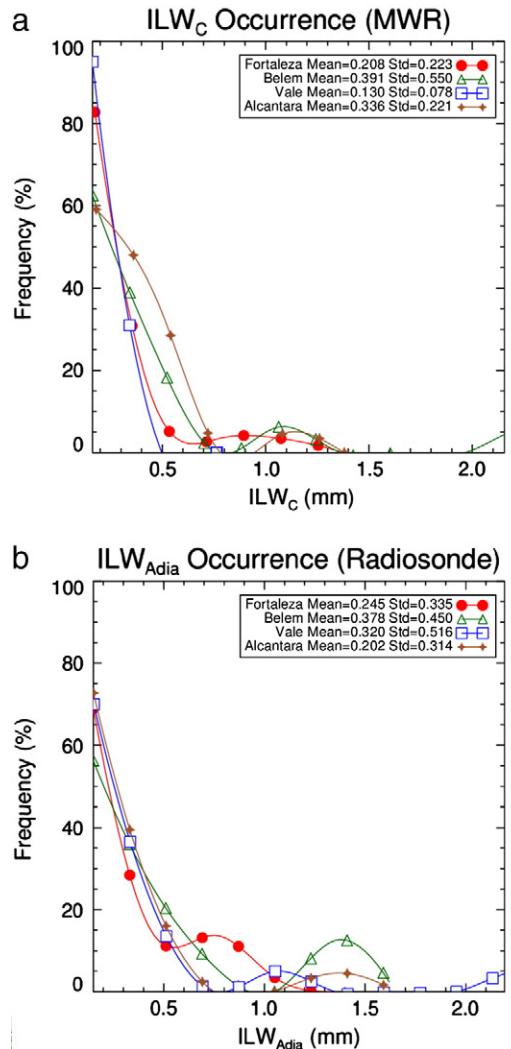


Fig. 2. The relative frequency histogram of the cloud liquid water content (mm) for all sites during the CHUVA campaign, estimated by (a) microwave ground-based radiometer (ILW_C) and (b) the adiabatic approach from radiosondes (ILW_{adia}).

Table 3

The cloud and rain liquid water contents from active and passive sensors for different regions and rainy systems in Brazil during the CHUVA campaign.

Integrated liquid water (mm)											
Site	Non-rainy			Rainy							
	ILW _C	MWR	ILW _{adia} radiosonde	MRR	XPOL			ILW _R (H _{LCL} – H _{0 °C-1km})			VIL
				General	Warm	Stratiform (BB ^a)	Deep convection			Mixed	Glaciated
Alcântara/MA	Mean	0.34	0.20	–	0.38	0.11	0.38	2.15		0.07	0.01
	Std	0.22	0.31	–	0.81	0.19	0.31	2.34		0.10	0.02
Fortaleza/CE	Mean	0.21	0.25	0.26	0.58	0.17	0.19	5.11		0.13	0.02
	Std	0.22	0.34	0.47	1.92	0.27	0.20	4.73		0.36	0.04
Belém/PA	Mean	0.39	0.38	0.45	0.38	0.10	0.15	2.61		0.20	0.08
	Std	0.55	0.45	0.75	0.91	0.18	0.11	1.60		0.49	0.20
Vale do Paraíba/SP	Mean	0.13	0.32	0.49	0.29	0.02	0.20	2.87		0.23	0.03
	Std	0.08	0.52	1.86	0.89	0.05	0.18	2.21		0.93	0.11
Warm rain	Mean			0.27	0.09						
	Std			0.90	0.19						
Stratiform (with BB)	Mean			0.21	0.22						
	Std			0.79	0.22						
Convective	Mean			2.35	3.60						
	Std			3.45	3.55						

^a BB – bright band.

highest LWC values were: $LWC_{ALC\grave{A}NTARA} = 10.1 \text{ g m}^{-3}$; $LWC_{FORTALEZA} = 10.4 \text{ g m}^{-3}$; $LWC_{BEL\acute{E}M} = 8.2 \text{ g m}^{-3}$; and $LWC_{VALE} = 11.6 \text{ g m}^{-3}$.

3. Results

3.1. Cloud liquid water

In order to compare the observed values of non-precipitating clouds by MWR with the measurements performed by radiosondes, an adiabatic approach was used. The mean ILW_C in a 3 h period before and after the launch of radiosonde (the highest temporal resolution of the radiosondes was 6 h) was used. This analysis represents the mean behavior of non-precipitating clouds with respect to

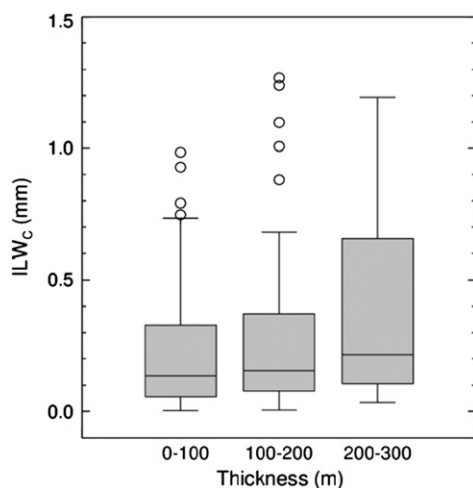


Fig. 3. The ILW_C (mm) estimated by the radiometer and the cloud thickness (m) estimated by the LiDAR for non-precipitating conditions at Fortaleza. Boxplot: Circles are the outliers; maximum and minimum values are the error bars; Lower part of the box corresponds to the 25th percentile and the upper part to the 75th percentile; the line inside the box corresponds to the median.

maximum liquid water content observed by the adiabatic process for each radiosonde. Fig. 2 shows the relative frequency histograms (smoothed curves) of (a) mean ILW_C and (b) ILW_{adia} for the four experiments. The statistics can be viewed in Table 3. For Fortaleza, 234 ILW_C cases were collocated and compared to 29 ILW_{adia} cases (radiosondes). For Alcântara only 79 ILW_C measurements were related to 23 ILW_{adia} values (the lowest MWR temporal resolution, each 6 min). Belém had the smallest sample with 17 ILW_{adia} values to compare with the collocated values of 115 ILW_C. However, Vale do Paraíba had the most expressive sample (the longest period of the measurements), with 1027 ILW_C related to 20 ILW_{adia}.

Table 3 shows the mean values, standard deviations and estimation methodology for each region. As shown in Fig. 2, the non-raining ILW_C distribution is similar among the four regions. Vale presents the most distinct behavior. Alcântara and Belém are characterized by proportionally more cloud liquid water content, as measured by MWR, than Fortaleza and Vale do Paraíba. Nevertheless, Belém and Fortaleza had the smallest differences between the two methodologies. In Alcântara and Belém, the mean value for ILW_C is close to 0.4 mm. Note that the Belém measurements present the largest variability and the average value is less representative. According to Löhnert and Crewell (2003), an ILW_C above 0.4 mm may be associated with the existence of raindrops that strongly affect the microwave brightness temperatures. According to Greene and Clark (1972), 90% of maritime warm clouds present drizzle when ILW_C is greater than 0.25 mm.

It is evident in Fig. 2a that, above 0.5 mm, the frequency is higher at the tropical sites. However, in the adiabatic distributions (Fig. 2b), the frequency of values above 0.5 mm is higher in comparison to the radiometer estimates in Belém and Vale do Paraíba. The lowest ILW_C amount was observed in Vale (see Table 3); on the other hand, its ILW_{adia} was one of the highest. In principle, the dry entrainment effect reduces the liquid water content more than that estimated by adiabatic processes (Jonas, 1996). One possible

Table 4

Occurrence (%), average (R_{Mean}) and standard deviation (R_{Std}) of rain rate for classified* rainy events ($R > 0.1 \text{ mm h}^{-1}$) over the main site for all CHUVA project experiments.

Site Type	Alcântara			Fortaleza			Belém			Vale		
	%	R_{Mean}	R_{Std}	%	R_{Mean}	R_{Std}	%	R_{Mean}	R_{Std}	%	R_{Mean}	R_{Std}
Stratiform (with BB ^a)	26	3.9	4.9	36	1.8	1.9	19	1.8	1.4	23	2.6	3.8
Convective	6	29.0	49.3	8	45.1	43.4	8	61.6	59.2	6	79.5	123.3
Warm	19	7.8	22.3	14	3.0	5.0	25	4.9	8.8	16	4.9	13.2
Other Class	49	6.5	13.3	43	2.6	5.9	48	8.6	17.2	55	8.6	60.9
Total sample	count	R_{Mean}	R_{Std}	count	R_{Mean}	R_{Std}	count	R_{Mean}	R_{Std}	count	R_{Mean}	R_{Std}
	155	7.6	18.9	360	5.7	17.1	104	10.4	25.0	458	10.8	56.9

*The statistics are only related to these 3 distinct rainy classes; other events can be identified but are not computed here, such as stratiform without a bright band, weak convective and warm with other clouds in upper levels.

^a BB – bright band.

reason is stronger dry entrainment in Vale do Paraíba, where drier air was reported. The mean integrated water vapor in Vale do Paraíba was 27 mm and at the other sites the value was higher than 43 mm.

For the Fortaleza experiment the LiDAR and ground-based radiometer systems were co-located to analyze the relationship between cloud thickness and the non-precipitating liquid water content. Only clouds with cloud base below the 0 °C were included. Fig. 3 shows boxplots with the values of liquid water for cumulus non-raining cloud thicknesses of 0–100 m, 100–200 m and 200–300 m. Specifically, one boxplot shows 50% of the ILW_C related to a specific thickness range, the lower part (lower quartile) of the box shows the 25th percentile, the upper part (upper quartile) is related to the 75th percentile and the line inside of the box is the median. We note that the median ILW_C in the boxes increases with cloud thickness. Furthermore, it is evident from the figure that there is greater variability in the values (indicated by an increased interquartile range) obtained for thicker clouds. In addition, there was a notable increase of the maximum value (line above the box) for thicker clouds. Few outliers (circle) were observed; however, 3 points larger than 1.5 mm, related to the last two thickness classes, were not shown for visualization purposes. It should be noted that only cloud thicknesses less than 300 m were considered in this analysis.

3.2. Rain liquid water

3.2.1. Integrated liquid water

This section analyzes the distribution of rain liquid water content, integrated up to 1 km below the freezing level. The total number of samples for each site can be seen in Table 4 (last line). Fig. 4 shows the distribution of the ILW_R measurements, estimated by (a) MRR and (b) XPOL, for the CHUVA sites. However, in Alcântara, MRR was not used in the vertical orientation; instead, it was employed at a slant, pointed toward the XPOL radar. ILW_R values above 1.5 mm were observed and were included in the statistical computations, although they are not shown in Fig. 4 due to their low frequency in comparison to the lower values. Upon the inspection of both figures, we note that the measurements are quite similar, despite the fact that the rainwater content in the analyzed layer is higher than that estimated by MRR when compared to the XPOL data for Vale and Belém. This result is expected, because MRR was a vertical profile at the main site and the XPOL was based on the RHI and probably

did not capture the first layers. Also, the strong downdraft associated with these deeper convective clouds could be the reason for the ILW_R overestimate (Tridon et al., 2011). The MRR measures the Doppler spectrum and estimate reflectivity based on the relationship between terminal velocity and droplet size. In addition, MRR has a large attenuation for strong rainfall events. The variability among both measurements does not allow the precise definition of regional differences.

Table 3 shows that the Fortaleza and Vale sites yielded the most significant differences between the MRR and XPOL data for the ILW_R estimation. This may be due to the presence of different DSDs observed for each location in the analyzed layer. Further details on the drop size distribution are given in later sections. Fig. 4 shows that the ILW_R distributions are generally similar among regions considering the large standard deviation compared with the mean value. However, some regional differences can be detailed. The highest average values were observed in Fortaleza, which had an average of 0.58 mm, followed by Belém and Alcântara. These high values may be associated with the high observed integrated water vapor, 44, 43 and 47 mm for Alcântara, Belém, and Fortaleza, respectively. The ILW_R value in Vale was lower than the other sites as already mentioned and expected, similar to the mid-latitude features.

In addition to the ILW_R values in the liquid cloud layer, the ice part of the cloud was also analyzed. VIL, Eq. (9), for the mixture and glaciated layers was calculated. The events observed in Vale do Paraíba and Belém regions (Table 3) yielded the highest values, because the convection over this region was the most intense, where the presence of squall lines and other convective systems was observed. Vale do Paraíba shows the most developed mixed layer (here defined as the layer from 0 to –20 °C) and Belém shows the highest VIL values in the glaciated cloud layer (here defined as the layer from –20 to –40 °C).

3.2.2. Integrated liquid water contents of the different cloud types

This section analyzes the average behaviors and distributions that are associated with the different types of precipitation, the classifications of deep convective, stratiform with bright band and warm clouds retrieved from the XPOL RHI profiles and the local radiosondes. The first classification level is associated with the identification of warm rain events for which the whole reflectivity profile must be below 0 °C. The next step is to identify the bright

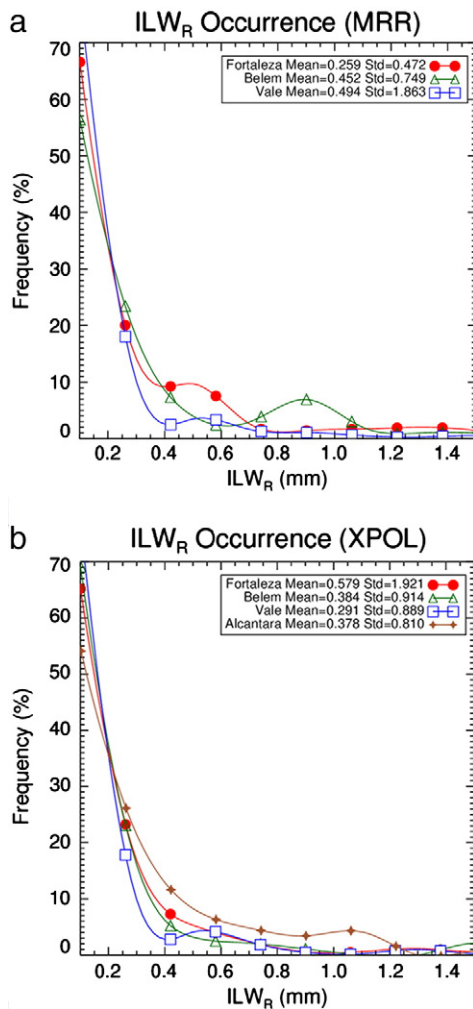


Fig. 4. The relative frequency histogram of the rain liquid water content (ILWR_R, mm) integrated up to 1 km below the 0 °C height for all sites during the CHUVA campaign, estimated by (a) MRR and (b) XPOL.

band in stratiform events based on the work of Fabry and Zawadzki (1995). The classification is applied as a function of the vertical variation of radar reflectivity (dBZ/km) and the polarimetric ρ_{HV} variable (the co-polar correlation coefficient), described by Zrníc et al. (1994). For a layer of 1 km above and below the 0 °C level (defined by the radiosonde), three different thresholds based on the mean and standard deviation of each of the analyzed variables are defined for each site under a control condition of pre-selected stratiform and convective events. If the BB is not found and the reflectivity is greater than the 39-dBZ threshold, then the system is classified as convective (Awaka et al., 2007). Clouds not fulfilling these conditions were not classified. The sample size of each class can be found in Table 4.

Table 3 shows that while warm and stratiform clouds had similar liquid water contents, the convective events had significantly higher values. The cloud type analysis also depends on the rain rate, therefore should be considered in a broad sense and supported by Table 4. The ILWR_R distributions for the three classes and for each site can be

observed in Fig. 5; except for convective clouds, the charts were limited to 2 mm. It can be observed in Fig. 5a that warm clouds show a similar regional distribution, but in Fig. 5b we note that Alcântara presents a different distribution. Alcântara shows stratiform clouds with a thicker liquid layer than the other regions. This can be associated with more active warm clouds that grow above the freezing level, thereby creating a thin layer of ice and becoming classified as stratiform clouds. Table 4 shows the frequency of events classified by each VPR (convective, stratiform with bright band and warm), related to rain rates equal to or higher than 0.1 mm h⁻¹; thus, the mean rain rate and standard deviations were also considered. Note that Table 4 refers to the specific cloud types described previously; clouds such as multilayers, high clouds, stratiform clouds without bright band and weak convective clouds ($Z < 39$ dBZ) are considered as “other” and represent at least 40% of the cases. It can be observed that Vale and Belém have the highest rainfall intensity for convective clouds and Alcântara has the highest mean/standard deviation values for warm and stratiform clouds. For the sites located in tropical regions, the liquid water content associated with warm clouds (Fig. 5a) was higher, in particular for sites near the coast, than the content observed in Vale do Paraíba, where the frequency of events with ILWR_R below 0.5 mm was greater. This is in agreement with Liu and Zipser (2009); they found a higher frequency of warm rain detectable by the TRMM satellite near the east coast of Brazil. The convective events have a good regional agreement except for Alcântara, which appears to have two populations of convective clouds (Fig. 5c). The convective clouds over Vale were observed to have high precipitation efficiency; that is, even with the lowest ILWR_R content, these clouds generated the highest rain rates (see Table 4).

3.2.3. Vertical LWC_R profiles for the different cloud types

In the previous section, we determined that an intrinsic relationship exists between the distributions of rain liquid water and the different types of precipitating events observed in each region. Our analysis of the vertical profiles of these distributions show which layer is more important within the analyzed systems, as well as how that layer varies. Fig. 6 shows the mean profiles of LWC_R (g m⁻³) for each site, as estimated by XPOL for warm, stratiform and convective clouds. Fig. 6 shows a significant regional difference, that is, to first order, a different average rain rate as described in Table 4. The profiles for lower rain rates are very similar; however, as the rain rate increases the profiles appear to be more different.

Fig. 6a shows, as already discussed, regional differences for the warm clouds in Vale do Paraíba. The mean profiles of the stratiform clouds (Fig. 6b) show that the bright band height observed near the coast is higher than that of the continental clouds. The mean freezing level is 4.9 km in Fortaleza and Alcântara, 4.5 km in Belém and 4.4 km in Vale do Paraíba. The warm processes in the coastal clouds would benefit from the presence of a larger layer at the coast than in the continental systems, which would consequently provide a comparatively longer time for droplet development, yielding larger droplets, which can be observed through the greater values of LWC_R in the higher layers for Fortaleza, Belém and Alcântara. As already mentioned, a significant

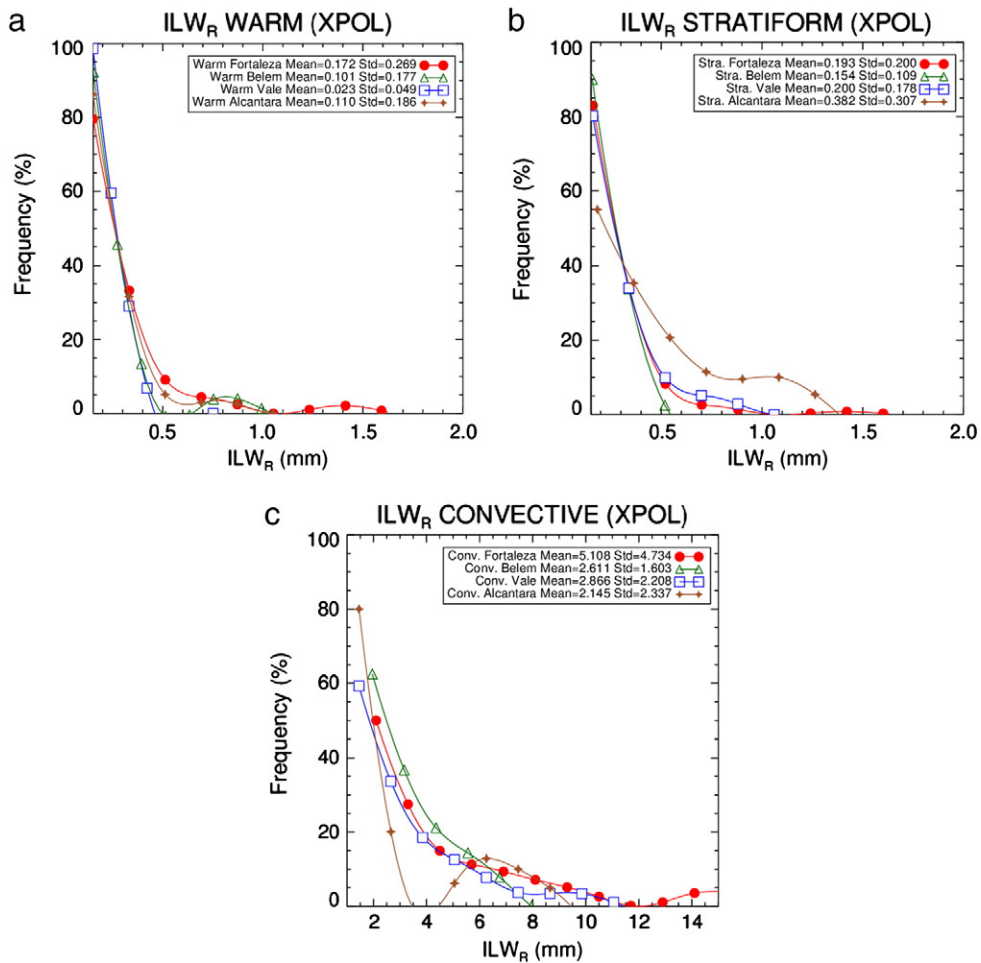


Fig. 5. The relative frequency histogram of the rain liquid water content (ILW_R , mm) integrated up to 1 km below the 0°C height estimated by XPOL for each site, related to (a) warm, (b) stratiform and (c) convective cloud types.

amount of liquid water was observed above 0°C in the stratiform clouds in Alcântara (Fig. 6b, line with stars). For convective clouds (Fig. 6c), Belém showed events with higher LWC_R in the glaciated layer, while Vale presented higher values in the mixed layer.

3.2.4. Surface raindrop size distribution

Understanding the DSD for the different systems over the sites is essential for rain characterization as well as for our understanding of the processes and differences among all of the previously analyzed distributions (Hu and Srivastava, 1995; Martins et al., 2010). It is well known that DSD varies with precipitation intensity, cloud type and location, and that even different measurement instruments at the same site sometimes provide different DSDs (Tokay and Short, 1996; Tokay et al., 2001; Caracciolo et al., 2006; Islam et al., 2012; Tokay et al., 2013). Fig. 7a, b, and c shows the average concentrations ($\text{m}^{-3}\text{mm}^{-1}$) of raindrops with respect to raindrop diameter (mm), as observed by the PARSIVEL disdrometer for all sites and rain classifications (size limited to 8.0 mm). These distributions confirm the previous results. With respect to warm clouds (Fig. 7a), Alcântara exhibited the largest droplets, while Vale had the highest concentration

of smaller raindrops, with these two locations demonstrating the highest and lowest rain rates, respectively. The warm clouds in Belém showed drops up to 5.5 mm in diameter, while Fortaleza yielded a maximum of approximately 4 mm, and in Alcântara, the maximum was nearly 8 mm. However, as mentioned previously, according to Tokay et al. (2013), the PARSIVEL disdrometer tends to overestimate the concentration of bigger raindrops. The distributions for the stratiform clouds (Fig. 7b) are usually similar. With respect to the convective DSDs (Fig. 7c), the largest droplets and concentrations formed by the intense systems in Belém and Vale are evident, and are less significant in Alcântara. Fortaleza showed an intermediary mean DSD, between that of Alcântara and Belém, which explains the high values of liquid water observed in the previous analyses in comparison to Alcântara and the lower rain rate compared to Belém. The distributions in Belém and Vale presented similarities up to 5.5 mm. Nevertheless, the biggest raindrop was observed for Vale clouds, which was the reason for the highest rain rate.

The contribution of each raindrop class to the total liquid water content was computed using the values of LWC_{D_i} (the LWC only for a particular drop, D_i) and the total LWC observed for each DSD. Fig. 7d, e, and f shows the diameter

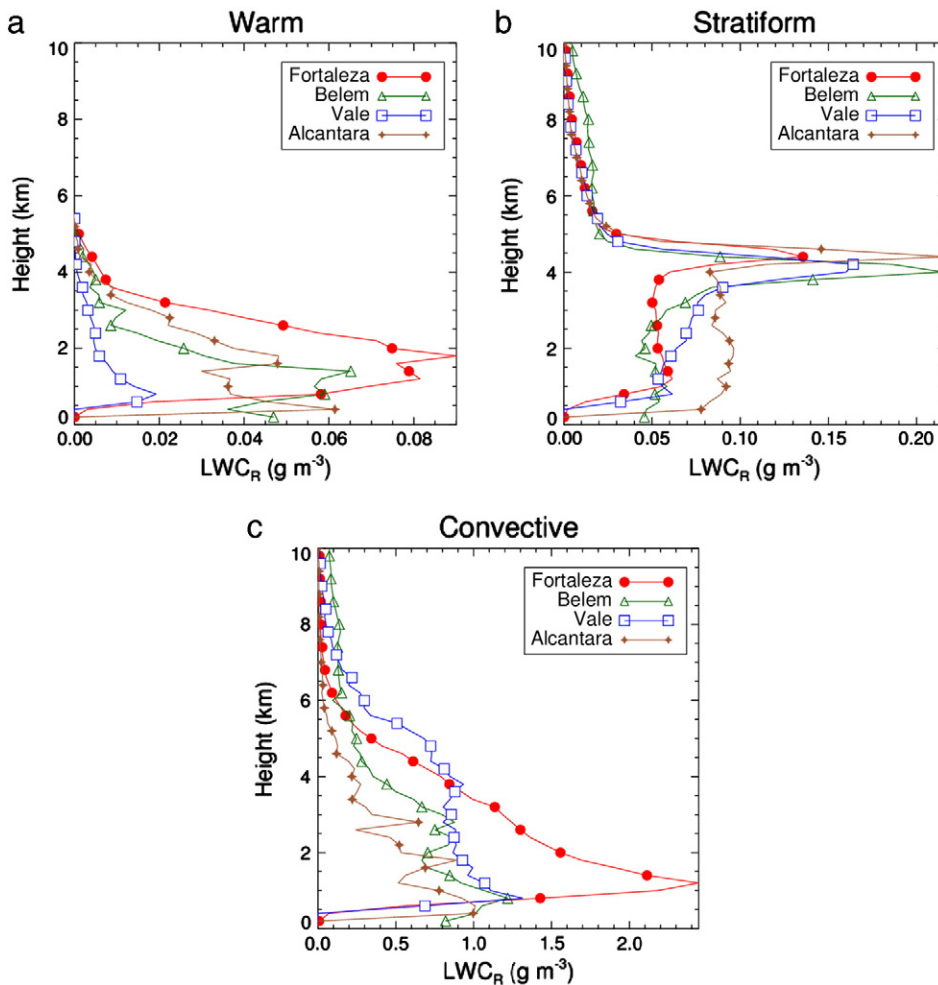


Fig. 6. The mean profile of the rain liquid water content (LWC_R , $g\ m^{-3}$) estimated by XPOL for each site, related to (a) warm, (b) stratiform and (c) convective cloud types.

contribution (%) for the LWC, based on each classification. Fig. 7d shows that the warm events in Vale do Paraíba are uniform, where an influence of different raindrops exists, probably related to the occurrence of different life cycles. In contrast, the events in Fortaleza are more highly associated with drops between 1 and 2 mm in diameter. Belém and Alcântara showed similar behaviors up to diameters of 3 mm, where the maximum was associated with drops measuring approximately 1.5 mm, which is the same size as for Fortaleza. Among the studied sites, Alcântara presented the most significant contribution of larger drops in the total liquid water content of warm clouds. Stratiform clouds (Fig. 7e) showed a similar distribution. However, there was a greater contribution of drops below 1.5 mm in size in Fortaleza and Vale, while above this diameter, the greatest contributions were obtained in Belém and Alcântara. The convective clouds (Fig. 7f) observed in Alcântara received greater contributions from raindrops measuring 2 and 3 mm, while at the other sites, larger raindrops were the most important. This result was particularly true in Belém and in Vale, where the highest rain rates were observed. For Fortaleza this is in agreement with the highest ILW_R .

3.2.5. Precipitation and mean ILW_R

Understanding the average behavior of the rain liquid water content according to its rainfall intensity is essential for determining relationships that can be applied for improvements in satellite precipitation estimations and numerical weather forecasting models. Fig. 8 shows the XPOL estimated ILW_R values for the events, classified according to their precipitation intensity, i.e., light (1 to $2.5\ mm\ h^{-1}$), moderate (2.5 to $10\ mm\ h^{-1}$), intense (10 to $50\ mm\ h^{-1}$) and severe rain (more than $50\ mm\ h^{-1}$). Three outlier points close to $16\ mm$ were observed for Fortaleza related to the last two classes but were omitted for the purpose of visualization. The values tend to increase gradually with the precipitation rate, and in some cases this increase is more pronounced, such as in Fortaleza. Our analyses of the rain intensity show that as the rain rate increases, the liquid water content also increases, specifically within the rain layer up to 1 km below the $0\ ^\circ C$ elevation. It is also worth noting that, in the light to moderate event classifications, a growth of the mean ILW_R values can be observed, even if small. This slope is steeper for the moderate to intense rainfalls, and increase with rainfall in the next

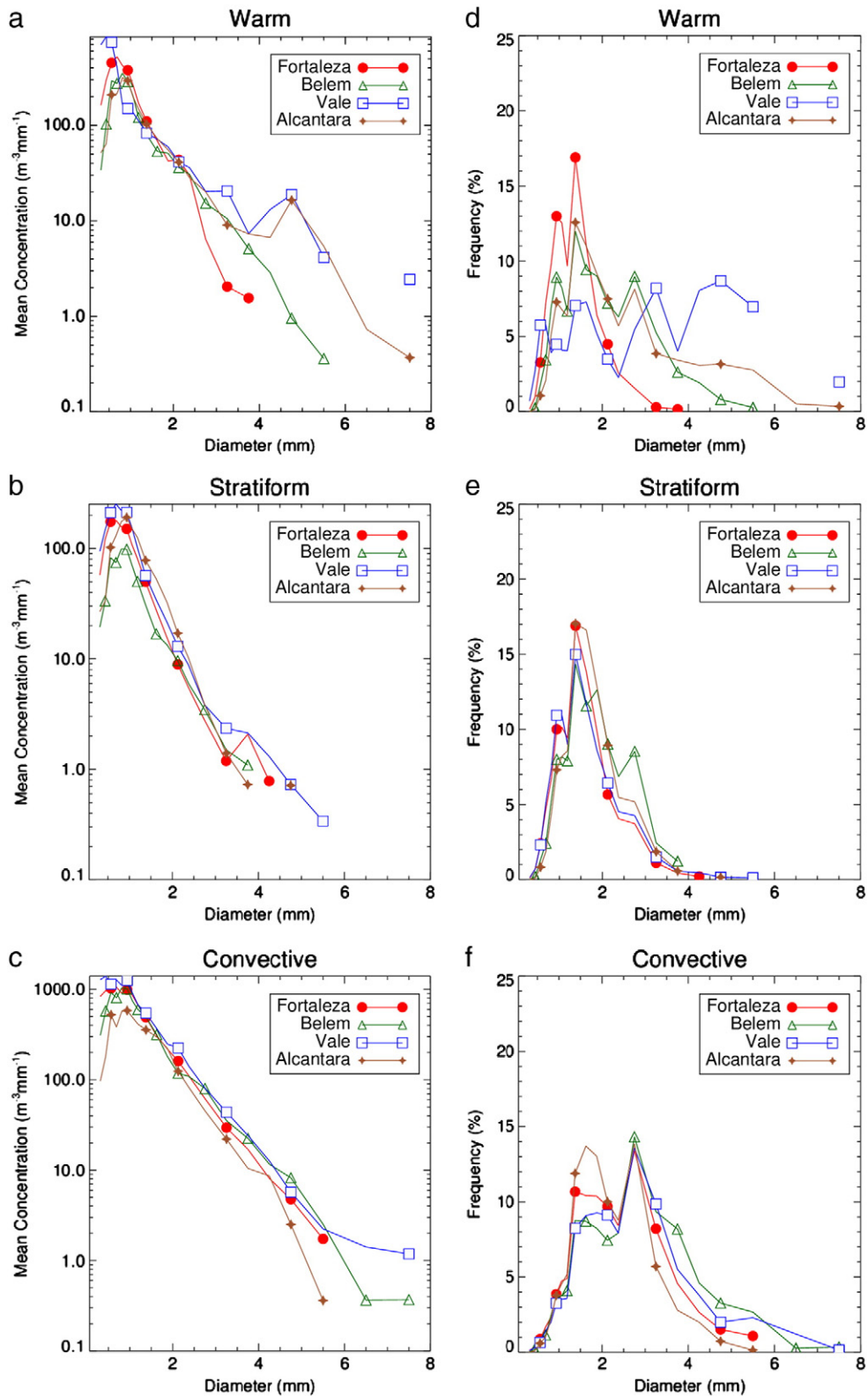


Fig. 7. The mean (a, b, and c) raindrop concentrations ($m^{-3} mm^{-1}$) and the frequency (%) of the liquid water content (d, e, and f) in relation with the total DSD for each diameter (D, in mm) for (a, d) warm, (b, e) stratiform and (c, f) convective clouds for the four sites.

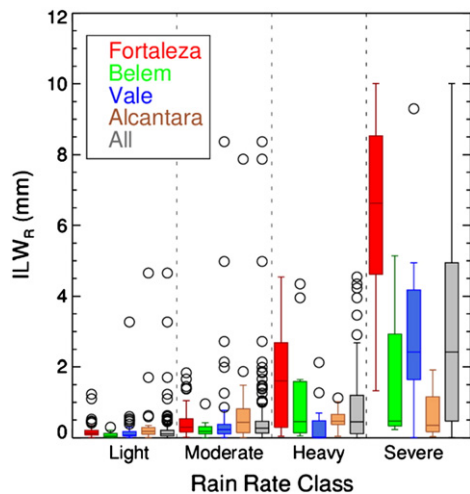


Fig. 8. The integrated rain liquid water (ILW_r , mm) estimated by XPOL for different rain intensities, including *light rain* (1 to 2.5 mm h^{-1}), *moderate rain* (2.5 to 10 mm h^{-1}), *heavy rain* (10 to 50 mm h^{-1}) and *severe rain* (larger than 50 mm h^{-1}) for all sites in the CHUVA campaign. Boxplot: as mentioned in Fig. 3.

class, which further increases the regional variability of the rainy systems. Most of the differences among sites and observed outlier points are related to the occurrence of different raining systems for the same rain rate.

4. Conclusion

This study compiles the rain and cloud data collected during four CHUVA experiments to describe the typical cloud and rainfall characteristics as functions of different instruments, cloud types (in a broad sense) and regions.

Different instrumentations and methodologies were compared in the description of the cloud and rain properties. Rain properties retrieved by MRR and XPOL, DSD from PARSIVEL and cloud liquid water from radiosondes and MWR were some of the examples of different instruments used to compute the same physical values. Particularities of each instrument or methodologies were described as well the procedures employed in order to have comparable physical information. A considerable variability among the different instruments was observed. These differences were sometimes useful for estimating the main physical processes involved in each situation. For instance, the adiabatic integrated liquid water content of clouds when compared to the microwave radiometer allowed the understanding of the larger effect of entrainment in Vale do Para iba clouds. In the MRR and the XPOL observations we can see the importance of vertical motions mainly in Bel em and Vale do Para iba.

Another reason for the variability found among the regions could be related to the different rainfall frequencies associated with the large scale fields. Some campaigns were associated with more intense and higher frequency deep convective precipitation events, others with more suppressed and shallower convection. Therefore, the average rain rate for each region is considerably different, as well the

maximum rain rate and the available water vapor. Thus, part of the regional differences found in this work was most likely due to the different rain rates observed, that are directly correlated to the total liquid water content.

The cloud classification for warm cloud, deep convective and stratiform cloud with BB takes into account only half of the total clouds. Multilayer clouds, stratiform clouds without BB, and probably warm clouds higher than the melting layer and towering cumulus clouds with weaker reflectivity can account for nearly 50% of the cloud population.

In addition to all this variability and the different samples, some interesting different regional and cloud type properties can be assigned. Vale do Para iba has the least intense warm clouds, most likely due to the entrainment effect, the largest population of continental aerosol (the most typically continental among the four sites) and the lowest integrated water vapor, reducing the liquid water content. For the other three sites significant differences cannot be assigned. The regional differences are only observed for high rain rates; for low rain rates the vertical profiles as well the integrated liquid water content have no significant differences for the same raining system. As the rain rate increases the warm, stratiform and convective clouds present some regional differences. For the warm clouds there is a clear difference between Vale do Para iba and the other three regions. The stratiform clouds are very similar except in Alc antara where the layer below the melting layer has much more water. Some BB heights and intensities also show regional differences. The stratiform clouds in the coastal regions presented bright bands closer to the melting layer than in the others regions. This is most likely due to the occurrence of faster ice melting here than in the regions where deep convective clouds are more pronounced. The convective clouds in Vale do Para iba exhibit more intense processes in the mixed layer than any other cloud types. This is possibly due to the large amount of supercooled water; several thunderstorm and hailstorms were reported. In Bel em, we found clouds with more important glaciated layers and high cloud tops.

With respect to raindrop size, it was noted that the DSDs for all regions are very similar for small–medium drop sizes, while the differences are more prominent for the largest droplets. The typical DSD for stratiform clouds presents no differences, but for warm and convective clouds the differences appear for droplets larger than 4 mm.

This study intends to give the first statistics about clouds and rainfall in Brazil based on data from field campaigns. Future campaigns, with longer periods such as the one year campaign in Manaus in 2014, will be very important for consolidating these results. The similarities as well as the differences among the regions and cloud types can be important for satellite precipitation estimation algorithms and the validation of cloud resolving models.

Acknowledgments

This work was supported by FAPESP grant No. 2009/15235-8 and CNPQ No. 140818/2011-1. We also thank the CHUVA campaign team for their efforts in helping with instrument function, in particular Riad Bourayou, Marc Schneebeli and Ali Tokay for helping us to define the LiDAR, Radiosonde, and Disdrometer retrievals, respectively. We are

particularly grateful for the valuable and constructive suggestions and review given by the anonymous reviewers.

References

- Atlas, D., 1954. The estimation of cloud parameters by radar. *J. Meteorol.* 11, 309–317.
- Awaka, J., Iguchi, T., Okamoto, K., 2007. Rain type classification algorithm. In: Levizzani, V., Bauer, P., Turk, F.J. (Eds.), *Measuring precipitation from space: EURAINSAT and the future*, pp. 213–224 (Netherlands).
- Battaglia, A., Kummerow, C., Shin, D.B., Williams, C., 2003. Constraining microwave brightness temperatures by radar brightband observations. *J. Atmos. Ocean. Technol.* 20 (6), 856–871.
- Battaglia, A., Saavedra, P., Morales, C.A., Simmer, C., 2011. Understanding three-dimensional effects in polarized observations with the ground-based ADMIRARI radiometer during the CHUVA campaign. *J. Geophys. Res.* 116 (D9), 1–17.
- Battan, L.J., 1973. *Radar Observation of the Atmosphere*. The University of Chicago Press, Chicago.
- Beard, K.V., Ochs III, H.T., 1993. Warm-rain initiation: an overview of microphysical mechanisms. *J. Appl. Meteorol.* 32, 608–625.
- Bourayou, R., Calheiros, A.J.P., Sakuragi, J., Miacci, M., Barbosa, H.J.M., Angelis, C.F., Machado, L.A.T., 2011. Vertical cloud structure over a north-eastern Brazilian coastal city using LIDAR, a microwave radiometer and a K-band hydrometeor profiler. *Workshop on LiDAR measurements in Latin America – VI WLMILA 6*, 2011, La Paz, Bolivia. *Proceedings. LFA-UMSA, La Paz*.
- Cadeddu, M.P., Liljegren, J.C., Turner, D.D., 2013. The atmospheric radiation measurement (ARM) program network of microwave radiometers: instruments, data, retrievals. *Atmos. Meas. Technol.* 6, 2359–2372.
- Campos, E., Ware, R., Joe, P., Hudak, D., 2014. Monitoring water phase dynamics in winter clouds. *Atmos. Res.* (in press).
- Caracciolo, C., Prodi, F., Uijlenhoet, R., 2006. Comparison between Pludix and impact/optical disdrometers during rainfall measurement campaigns. *Atmos. Res.* 82 (Issues 1–2), 137–163.
- Cimini, D., Westwater, E.R., Han, Y., Keihm, S.J., 2003. Accuracy of ground-based microwave radiometer and balloon-borne measurements during WVOP2000 field experiment. *IEEE Trans. Geosci. Remote Sens.* 41, 2605–2615.
- Cimini, D., Campos, E., Ware, R., Albers, S., Giuliani, G., Oreamuno, J., Joe, P., Koch, S., Cober, S., Westwater, E., 2011. Thermodynamic atmospheric profiling during the 2010 Winter Olympics using ground-based microwave radiometry. *IEEE Trans. Geosci. Remote Sens.* 49 (12), 4959–4969.
- Cotton, W.R., Bryan, G.H., Van den Heever, S.C., 2010. *Storm and Cloud Dynamics*, 2nd ed., 99. Academic Press, Burlington, MA.
- Crewell, S., Löhnert, U., 2003. Accuracy of cloud liquid water path from ground-based microwave radiometry: 2. Sensor accuracy and synergy. *Radio Sci.* 38 (3), 8042.
- Czekala, H., Simmer, C., 1998. Microwave radiative transfer with nonspherical precipitating hydrometeors. *J. Quant. Spectrosc. Radiat. Transf.* 60 (3), 365–374.
- Czekala, H., Crewell, S., Simmer, C., Thiele, A., 2001. Discrimination of cloud and rain liquid water path by groundbased polarized microwave radiometry. *Geophys. Res. Lett.* 28 (2), 267–270.
- Donaldson, R.J., 1955. The measurement of cloud liquid-water content by radar. *J. Meteorol.* 12, 238–244.
- Doviak, R.J., Zrnic, D.S., 1993. *Doppler Radar and Weather Observations*, 2nd ed. Courier Dover Publications, New York.
- Ebell, K., Löhnert, U., Crewell, S., Turner, D.D., 2010. On characterizing the error in a remotely sensed liquid water content profile. *Atmos. Res.* 98 (Issue 1), 57–68.
- Eccles, P.J., Mueller, E.A., 1971. X-band attenuation and liquid water content estimation by a dual-wavelength radar. *J. Appl. Meteorol.* 10, 1252–1259.
- Fabry, F., Zawadzki, I., 1995. Long-term radar observations of the melting layer of precipitation and their interpretation. *J. Atmos. Sci.* 52, 838–851.
- Gonzalez, R.C., Woods, R.E., Eddins, S.L., 2009. *Digital Image Processing Using MATLAB 2*. Gatesmark Publishing, Knoxville.
- Greene, D.R., Clark, R.A., 1972. Vertically integrated liquid water – a new analysis tool. *Mon. Weather Rev.* 100, 548–552.
- Hagen, M., Yuter, S.E., 2003. Relations between radar reflectivity, liquid-water content, and rainfall rate during the MAP SOP. *Quart. J. R. Meteorol. Soc.* 129, 477–493.
- Han, Y., Westwater, E.R., 2000. Analysis and improvement of tipping calibration for ground-based microwave radiometers. *IEEE Trans. Geosci. Remote Sens.* 38 (Issue 3), 1260–1276.
- Hardy, W.N., 1973. Precision temperature reference for microwave radiometry. *IEEE Trans. Microw. Theory* 21, 149–150.
- Hewison, T.J., 2006. *Profiling temperature and humidity by ground-based microwave radiometers*. PhD Thesis University of Reading.
- Hogan, R.J., Gaussiat, N., Illingworth, A.J., 2005. Stratocumulus liquid water content from dual-wavelength radar. *J. Atmos. Ocean. Technol.* 22, 1207–1218.
- Houze Jr., R.A., 1993. *Cloud Dynamics*. Academic Press, San Diego.
- Hu, Z., Srivastava, R.C., 1995. Evolution of raindrop size distribution by coalescence, breakup, and evaporation: theory and observations. *J. Atmos. Sci.* 52, 1761–1783.
- Ingold, T., Peter, R., Kämpfer, N., 1998. Weighted mean tropospheric temperature and transmittance determination at millimeter-wave frequencies for ground-based applications. *Radio Sci.* 33, 905–918.
- Islam, T., Rico-Ramirez, M.A., Thurai, M., Han, D., 2012. Characteristics of raindrop spectra as normalized gamma distribution from a Joss-Waldvogel disdrometer. *Atmos. Res.* 108, 57–73.
- Jaffrain, J., Berne, A., 2011. Experimental quantification of the sampling uncertainty associated with measurements from PARSIVEL Disdrometers. *J. Hydrometeorol.* 12, 352–370.
- Jonas, P.R., 1996. Turbulence and cloud microphysics. *Atmos. Res.* 40 (2), 283–306.
- Joss, J., Waldvogel, A., 1967. Ein Spectrograph für Niederschlagstropfen mit automatischer Auswertung (A spectrograph for the automatic analysis of raindrops). *Pure and Applied Geophysics* 68, 240–246.
- Karmakar, P.K., Maiti, M., Sett, S., Angelis, C.F., Machado, L.A.T., 2011. Radiometric estimation of water vapor content over Brazil. *J. Adv. Space Res.* 28, 1506–1514.
- Kousky, V.E., Gan, M.A., 1981. Upper tropospheric cyclonic vortices in the tropical South Atlantic. *Tellus* 36 (6), 538–551.
- Lawson, R.P., Blyth, A.M., 1998. A comparison of optical measurements of liquid water content and drop size distribution in adiabatic regions of Florida cumuli. *Atmos. Res.* 47–48, 671–690.
- Liljegren, J.C., Clothiaux, E.E., Mace, G.G., Kato, S., Dong, X., 2001. A new retrieval for cloud liquid water path using a ground-based microwave radiometer and measurements of cloud temperature. *J. Geophys. Res.* 106 (D13), 14485–14500.
- Liu, C., Zipser, E.J., 2009. “Warm Rain” in the tropics: seasonal and regional distributions based on 9 year of TRMM Data. *J. Clim.* 22, 767–779.
- Löffler-Mang, M., Joss, J., 2000. An optical disdrometer for measuring size and velocity of hydrometeors. *J. Atmos. Ocean. Technol.* 17 (2), 130–139.
- Löhnert, U., Crewell, S., 2003. Accuracy of cloud liquid water path from ground-based microwave radiometry 1. Dependency on cloud model statistics. *Radio Sci.* 38, 8041.
- Löhnert, U., Crewell, S., Simmer, C., Macke, A., 2001. Profiling cloud liquid water by combining active and passive microwave measurements with cloud model statistics. *J. Atmos. Ocean. Technol.* 18, 1354–1366.
- Machado, L.A.T., Silva Dias, M.A.F., Morales, C., Fisch, G., Vila, D., Albrecht, R., Goodman, S.J., Calheiros, A.J.P., Biscaro, T., Kummerow, C., Cohen, J., Fitzjarrald, D., Nascimento, E., Sakamoto, M., Cunningham, C., Chaboureaud, J.-P., Petersen, W.A., Adams, D., Baldini, L., Angelis, C.F., Sapucci, L.F., Salio, P., Barbosa, H.M.J., Landolfo, E., Souza, R.F., Blakeslee, R.J., Bailey, J., Freitas, S., Lima, W.F., Tokay, A., 2014. The CHUVA Project – how does convection vary across Brazil? *Bull. Am. Meteorol. Soc.* (in press)
- Martins, C.R., Machado, L.A.T., Costa, A.A., 2010. Characterization of the microphysics of precipitation over Amazon region using radar and disdrometer data. *Atmos. Res.* 96 (Issues 2–3), 388–394.
- Mätzler, C., Morland, J., 2009. Refined physical retrieval of integrated water vapor and cloud liquid for microwave radiometer data. *IEEE Trans. Geosci. Remote Sens.* 47 (6), 1585–1594.
- Meywerk, J., Quante, M., Sievers, O., 2005. Radar based remote sensing of cloud liquid water – application of various techniques – a case study. *Atmos. Res.* 75 (Issue 3), 167–181.
- Michaelides, S., Levizzani, V., Anagnostou, E., Bauer, P., Kasparis, T., Lane, J.E., 2009. Precipitation: measurement, remote sensing, climatology and modeling. *Atmos. Res.* 94 (Issue 4), 512–533.
- Peter, R., Kämpfer, N., 1992. Radiometric determination of water vapor and liquid water and its validation with other techniques. *J. Geophys. Res.* 97 (D16), 18173–18183.
- Peters, G., Fischer, B., Münster, H., Clemens, M., Wagner, A., 2005. Profiles of raindrop size distributions as retrieved by microrain radars. *J. Appl. Meteorol.* 44, 1930–1949.
- Peters, G., Fischer, B., Clemens, M., 2010. Rain attenuation of radar echoes considering finite-range resolution and using drop size distributions. *J. Atmos. Ocean. Technol.* 27 (5), 829–842.
- Pruppacher, H.R., Klett, J.D., 1997. *Microphysics of Clouds and Precipitation*, 2nd Edn. Kluwer Academic Publishers, Boston.
- Rose, T., Crewell, S., Löhnert, U., Simmer, C., 2005. A network suitable microwave radiometer for operational monitoring of the cloudy atmosphere. *Atmos. Res.* 75, 183–200.
- Rossow, W.B., Schiffer, R.A., 1999. Advances in understanding clouds from ISCCP. *Bull. Am. Meteorol. Soc.* 80, 2261–2287.
- Saavedra, P., Battaglia, A., Simmer, C., 2012. Partitioning of cloud water and rainwater content by ground-based observations with the Advanced

- Microwave Radiometer for Rain Identification (ADMIRARI) in synergy with a micro rain radar. *J. Geophys. Res.* 117, 1984–2012.
- Satyamurthy, P., Nobre, C.A., Silva Dias, P.L., 1998. South America. In: Karoly, D.J., Vicent, D.G. (Eds.), *Meteorology of the Southern Hemisphere*. Amer. Meteorol. Soc., Meteorol. Monogr., 27(49), pp. 119–139.
- Schneebeil, M., Sakuragi, J., Biscaro, T., Angelis, C.F., Carvalho da Costa, I., Morales, C., Baldini, L., Machado, L.A.T., 2012. Polarimetric X-band weather radar measurements in the tropics: radome and rain attenuation correction. *Atmos. Meas. Tech.* 5, 2183–2199.
- Skou, N., Vine, D., 2006. *Microwave Radiometer Systems: Design and Analysis*, 2nd ed. Artech House, Norwood, MA.
- Smith, E., Asrar, G., Furuhashi, Y., Ginati, A., Kummerow, C., Levizzani, V., Mugnai, A., Nakamura, K., Adler, R., Casse, V., Cleave, M., Debois, M., Durning, J., Entin, J., Houser, P., Iguchi, T., Kakar, R., Kaye, J., Kojima, M., Lettenmaier, D.P., Luther, M., Mehta, A., Morel, P., Nakazawa, T., Neeck, S., Okamoto, K., Oki, R., Raju, G., Shepherd, M., Stocker, E., Testud, J., Wood, E. F., 2007. The international global precipitation measurement (GPM) program and mission: An overview. In: Levizzani, V., Bauer, P., Turk, F.J. (Eds.), *Measuring precipitation from space: EURAINSAT and the future*, pp. 611–653 (Netherlands).
- Solheim, F., Godwin, J., Westwater, E.R., Han, Y., Keihm, S., Marsh, K., Ware, R., 1998. Radiometric profiling of temperature, water vapor, and liquid water using various inversion methods. *Radio Sci.* 33, 393–404.
- Stephens, G.L., Kummerow, C.D., 2007. The remote sensing of clouds and precipitation from space: a review. *J. Atmos. Sci.* 64, 3742–3765.
- Testud, J., Bouar, E. Le, Obligis, E., Ali-Mehenni, M., 2000. The rain profiling algorithm applied to polarimetric weather radar. *J. Atmos. Ocean. Technol.* 17, 322–356.
- Tokay, A., Short, D.A., 1996. Evidence from tropical raindrop spectra of the origin of rain from stratiform versus convective clouds. *J. Appl. Meteorol.* 35, 355–371.
- Tokay, A., Kruger, A., Krajewski, W.F., 2001. Comparison of drop size distribution measurements by impact and optical disdrometers. *J. Appl. Meteorol.* 40, 2083–2097.
- Tokay, A., Petersen, W.A., Gatlin, P., Wingo, M., 2013. Comparison of raindrop size distribution measurements by collocated disdrometers. *J. Atmos. Ocean. Technol.* 30, 1672–1690.
- Tridon, F., Van Baelen, J., Pointin, Y., 2011. Aliasing in Micro Rain Radar data due to strong vertical winds. *Geophys. Res. Lett.* 38, L02804.
- Ware, R., Carpenter, R., Guldner, J., Liljegren, J., Nehrkorn, T., Solheim, F., Vandenberghe, F., 2003. A multichannel radiometric profiler of temperature, humidity, and cloud liquid. *Radio Sci.* 38, 8079.
- Ware, R., Cimini, D., Campos, E., Giuliani, G., Albers, S., Nelson, M., Koch, S.E., Joe, P., Cober, S., 2013. Thermodynamic and liquid profiling during the 2010 Winter Olympics. *Atmos. Res.* 132–133, 278–290.
- Westwater, E.R., 1993. Ground-based microwave remote sensing of meteorological variables. In: Janssen, M. (Ed.), *Atmospheric Remote Sensing by Microwave Radiometry*. John Wiley, New York, pp. 145–213.
- Westwater, E.R., Crewell, S., Matzler, C., Cimini, D., 2005. Principles of surface-based microwave and millimeter wave radiometric remote sensing of the troposphere. *Quat. Soc. Ital. Elettromagnetismo* 1 (50–90), 8041.
- Won, H.Y., Kim, Y.-H., Lee, H.S., 2009. An application of brightness temperature received from a ground-based microwave radiometer to estimation of precipitation occurrence and rainfall intensity. *Asian Pac. J. Atmos. Sci.* 45 (1), 55–69.
- Xu, G., Ware, R., Zhang, W., Feng, G., Liao, K., Liu, Y., 2013. Effect of off-zenith observations on reducing the impact of precipitation on ground-based microwave radiometer measurement accuracy in Wuhan. *Atmos. Res.* 2013.
- Zhao, Q., Carr, F.H., 1997. A prognostic cloud scheme for operational NWP models. *Mon. Weather Rev.* 125, 1931–1953.
- Zhao, L., Weng, F., 2002. Retrieval of ice cloud parameters using the advanced microwave sounding unit. *J. Appl. Meteorol.* 41, 384–395.
- Zhao, G., Chu, R., Zhang, T., Jia, W., 2013. Rainwater content estimated using polarimetric radar parameters in the Heihe River Basin. *Atmos. Res.* 120–121, 155–161.
- Zrnica, D.S., Raghavan, R., Chandrasekar, V., 1994. Observations of copolar correlation coefficient through a bright band at vertical incidence. *J. Appl. Meteorol.* 33, 45–52.